Journal of the Mechanics and Physics of Solids 58 (2010) 1571–1581

Contents lists available at ScienceDirect

Journal of the Mechanics and Physics of Solids

journal homepage: www.elsevier.com/locate/jmps

Discrete contact mechanics of a fibrillar surface with backing layer interactions

G.M. Guidoni [a], D. Schillo [a], U. Hangen [b], G. Castellanos [a], E. Arzt [a], R.M. McMeeking [a,c], R. Bennewitz [a,*]

[a] INM—Leibniz Institute for New Materials and Saarland University, Campus D2 2, 66123 Saarbrücken, Germany
[b] Hysitron, Inc., 10025 Valley View Road, Minneapolis, MN 55344, USA
[c] Department of Mechanical Engineering, University of California, Santa Barbara, CA 93106, USA

ARTICLE INFO

Article history:
Received 2 February 2010
Received in revised form
24 June 2010
Accepted 12 July 2010

Keywords:
Adhesion and adhesives
Mechanical testing
Viscoelastic material
Microstructures
Poly(dimethyl siloxane) (PDMS)

ABSTRACT

The contact mechanics of a fibrillar micro-fabricated surface structure made of poly(dimethyl siloxane) (PDMS) is studied. The attachment and detachment of individual fibrils to and from a spherical indenter upon approach and retraction are detected as jumps in force and stiffness. A quantitative model describes the stiffness values by taking into account the deformation of the fibrils and the backing layer. The results emphasize the importance of long-range interactions in the contact mechanics of elastic materials and confirm some of the important concepts underlying the development of fibrillar adhesive materials.

1. Introduction

Fibrillar microstructures of elastic materials interacting with substrates by short-range molecular forces, such as van der Waals attraction, have recently attracted attention as dry adhesives (Arzt et al., 2003; Boesel et al., in press; Del Campo and Arzt, 2008; Del Campo et al., 2007; Gorb et al., 2007; Greiner et al., 2007; Huber et al., 2005; Kim and Sitti, 2006; Lee et al., 2007; Peressadko and Gorb, 2004). Their development is motivated by the study of adhesion in biological systems exemplified by the feet of some insects and geckos (Arzt et al., 2003; Autumn, 2006; 2007; Autumn, et al., 2000; Huber et al., 2005; Sun et al., 2005). Such fibrillar architectures exhibit high adhesive strengths for a variety of reasons that have been summarized by Majumder et al. (2010) and subsequently by Kamperman et al. (2010). Such reasons include a higher peeling resistance, better conformation to rough surfaces, strengthening due to contact splitting (Arzt et al., 2003), the achievement of maximum van der Waals adhesive strength for a given area in contact (Gao and Yao, 2004), and better defect tolerance (Hui et al., 2004; McMeeking et al., 2008; Spuskanyuk et al., 2008).

Many of the systems that have been developed so far are produced by an integrated moulding process involving an elastomer, so that the fibrils are backed by a layer of the same elastic material. Efforts have been made to understand the pull-off mechanics of such systems. Long et al. (2008) used an elastic foundation to model the deformation of the fibril array while the deformation of the finite backing layer was modelled using linear elasticity theory. They found out that the normalized pull-off force is inversely proportional to both the thickness of the backing layer and the radius. Long and Hui

* Corresponding author. Tel.: +49 681 9300 213; fax: +49 681 9300 242.
E-mail address: roland.bennewitz@inm-gmbh.de (R. Bennewitz).

0022-5096/$ - see front matter © 2010 Elsevier Ltd. All rights reserved.
doi:10.1016/j.jmps.2010.07.009

(2009) used a similar approach with fibrils modelled as an elastic layer, and predicted the pull-off force for a prismatic circular indenter. They deduced that the pull-of force for a compliant backing layer should be less than that for a stiff one. Furthermore, Kim et al. (2007) modelled their fibrillar system as a foundation consisting of elastic springs between the rigid indenter and a backing layer. They focused mainly on the situation where a large number of fibrils are in contact. They found that very thin backing layers promote equal load sharing, maximizing adhesion. In the other extreme, very thick backings can lead to reduced adhesion, because of edge stress concentration similar to a rigid punch in adhesive contact with a half space. Noderer et al. (2007) observed an enhanced work of adhesion during the detachment of a glass indenter from an array of film-terminated fibrils, and deduced that the enhancement arose due to detachment trapping within the fibrillar system. In addition, they developed a successful model for the compliance of the film-terminated fibrillar array, deduced from the integrated effect of a large number of discrete fibrils.

In this study, following Noderer et al. (2007), we quantify the combined elastic response of fibrils and backing layer, and show that the measured stiffness of the system is strongly influenced by elastic deformations of the backing layer, even for the small strain deformations applied. Such long-range deformation of the substrate is an essential ingredient in recent models of the mechanical response of elastic systems (Persson, 2001). We focus mainly on the approach of a stiff sphere into contact with a fibrillar system, addressing this phenomenon with both experiments and a model. The high sensitivity of a nanoindenter allows us to register the sequence of attachment of individual fibrils. Investigating attachment, rather than detachment, allows us to avoid the non-linear effects of large strain and viscoelastic response, which often hamper the quantitative analysis of adhesion experiments involving elastomers. In our model we describe the combined deformation of fibrils and backing layer in a linear elastic analysis at small strains, as pioneered by Noderer et al. (2007). The combination of experiment and model allows us to understand the measured stiffness as a function of the number of fibrils in contact and to determine the elastic modulus of our material by in-situ measurements on individual fibrils on the backing layer. Finally we briefly discuss the compliance identified in experiments during retraction of the indenter, and extend our model for a single fibril in contact to include finite strains, observed during retraction.

2. Materials and methods

The PDMS samples, pillars integrated with the backing layer, were prepared using a soft-moulding process. A 10:1 ratio of Sylgard 184 prepolymer and cross-linker was mixed, degassed, and poured on a silanized SU-8 pattern containing cylindrical holes in a hexagonal packing arrangement. The mould was previously covered by a fluorinated polymer layer to favor the separation of the polymeric material. After curing at 60 °C and 600 mbar, during 24 h, the material was carefully demoulded, to obtain a structured PDMS surface on top of the backing layer. The tested area consisted of an arrangement of 7 fibrils of radius a=5 μm each and of height H=18.7 μm, measured by means of a white light interferometer (Zygo New View 5010). They are arranged in a hexagonal pattern; separated by a distance s_{ij}=20 μm between the centre of neighbouring fibrils with nos. i and j (see Fig. 1 for a schematic top view). The backing layer is 2.5 ± 0.3 mm thick.

Nanoindentation tests were carried out using a TI 900 instrument with a Performech controller (Hysitron TriboIndenter, Hysitron Inc., Minneapolis, MN, USA). A spherical sapphire indenter (radius $R \approx 348$ μm) was used. The radius of the sphere was calibrated through a series of indents into polycarbonate (PC) with a maximum penetration depth of 140 nm. The radius was confirmed by means of imaging with an optical microscope, and also by scanning a cube-corner indenter tip under imaging mode with the above mentioned instrument (TI 900). Fig. 2 is a schematic of the cross-section of the centre fibril and two of its closest neighbours. Note the large radius of curvature of the indenter tip compared to the diameter of the fibrils. The contact between each fibril and the indenter can be described as a local "flat punch" contact.

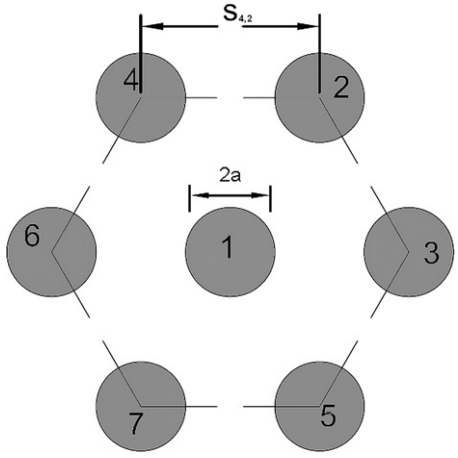

Fig. 1. Schematic top view of the hexagonal fibril arrangement. The fibrils have a radius of a=5 μm and a centre-to-centre distance between neighbours of s_{ij}=20 μm.

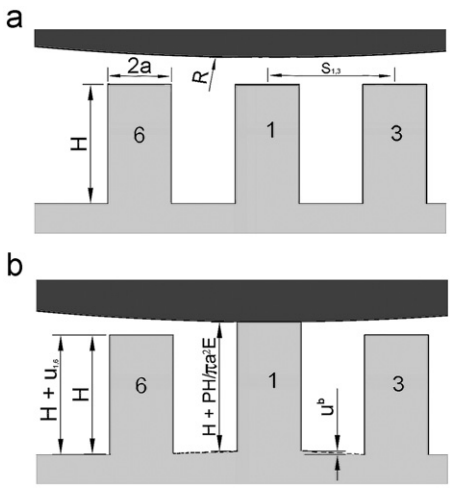

Fig. 2. (a) Cross-section of the centre fibril, two neighbours, and the indenter. The fibrils have a height of H=18.7 μm, the indenter a radius of R=348 μm. The scheme represents the situation where there is no interaction between indenter and fibrils. (b) Cross-section of the centre fibril, two neighbours, and the indenter just after attachment of the centre fibril to the indenter by long-range attractive forces. The scheme shows the elongation of the centre fibril, the deformation of the backing, and the resulting upward displacement of the neighbouring fibrils. The deformation is exaggerated for better visualization.

By means of an optical microscope, the indenter was approximately located above the centre fibril. The approach was done from a height where there was no contact and where no attractive or repulsive forces were registered. All measurements were done under displacement control, at an approach and retraction rate of 200 nm/s using a close-loop feedback displacement control.

3. Experimental results

Fig. 3 shows typical load–displacement curves for approach and retraction into a flat region and into a region with a hexagonal fibril structure on the same PDMS sample. The shape of the approach–retract curve recorded for flat PDMS has the curvature and the large hysteresis expected for indentation into an elastomer (e.g. see Fig. 1 in Ebenstein and Wahl (2006)). The curve recorded for the fibrillar structure generally resembles that for the flat surface, but with interesting differences. The individual attachment and detachment of the seven fibrils can be recognized through sudden jumps in the force. The attachment of the first fibril upon approach always generated a force drop into tension. This can be seen more clearly in Fig. 4, which is the approach curve shown on an enlarged scale. Subsequent to the first jump into contact, the curve is composed of linear sections with different slopes separated by force jumps. As we will discuss later in detail, this observation reflects step-wise increments in contact area. While the maximum tensile force during retraction is similar for the flat and the structured regions, the adhesion hysteresis, i.e. the area between the approach and retraction curves representing energy dissipated, is just over three times larger for the structured sample compared to the flat case.

The maximum penetration depth registered over all experiments on the structured sample was 1.4 μm, where this distance indicates how far into the fibrillar array the sphere was pressed. When its lowest point is 1.4 μm below the fibril tips, those as far away radially as 31 μm from the lowest point of the sphere will come into contact with the sphere. The group of seven fibrils on the sample is circumscribed by a circle of 25 μm in radius, and therefore we expect to make contact progressively with all seven fibrils in the course of approach.

In Fig. 4 each force jump upon approach has been numbered for clarity, corresponding to consecutive contact formation with individual fibrils. The increasing slope of the linear sections separating the force jumps quantifies the increments in the stiffness of the system as fibrils progressively make contact. Correspondingly, a decrease in slope between force jumps is observed in the retraction data (see Fig. 3) as the number of fibrils in contact decreases.

The stiffness (k_i) of the pillar structure (fibrils and backing), where i is the number of fibrils in contact, was determined for each section of the curve by linear fitting. Table 1 summarizes the average stiffness values from a series of approach curves. While the stiffness does increase monotonically, it does not scale linearly with the number of fibrils in contact as would be expected if the fibrils were acting as independent identical springs in parallel. The stiffnesses during retraction were also evaluated, and are shown in Table 2. The stiffness values during retraction differ from those found for the same number of fibrils in contact during approach. In particular, when there is only one fibril attached, the stiffness during retraction is almost exactly half that during approach; note that the force applied to a single fibril during retraction is about

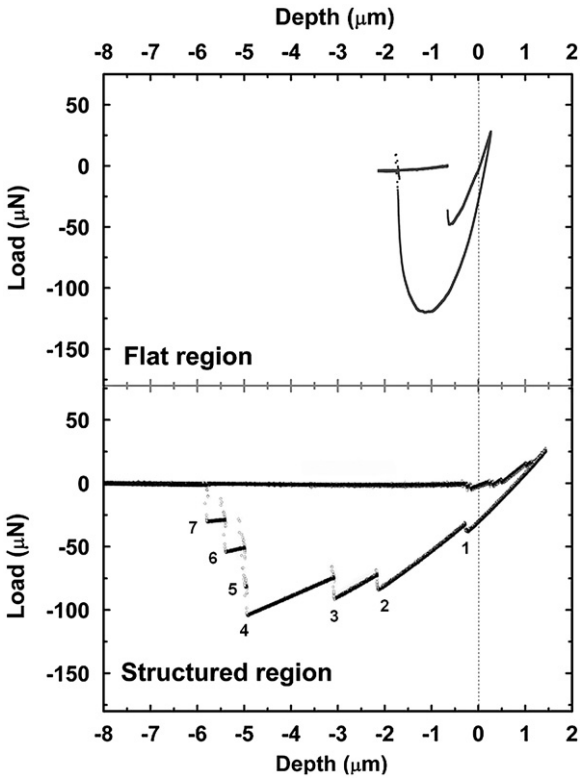

Fig. 3. Load vs. depth curve for approach and retraction on a PDMS sample. The upper graph is recorded on flat region of the sample while the bottom graph is recorded on a fibril structure as depicted in Fig. 1 of the same sample. For the structured sample, the detachment of individual fibrils is numbered in the order of occurrence.

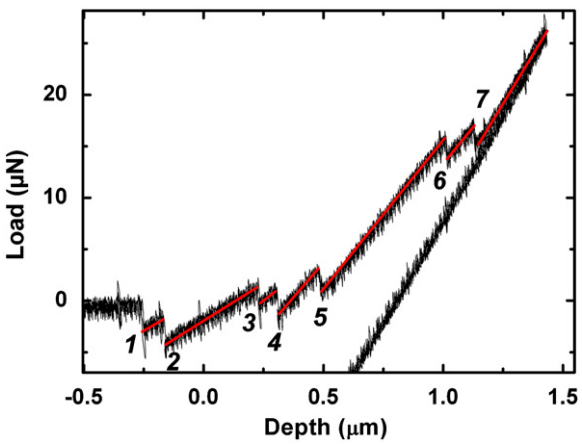

Fig. 4. Magnified view of the approach data of the load vs. depth curve for the fibril structure presented in Fig. 3. The seven force jumps indicate the attachment of individual fibrils. Red linear fitting curves were superimposed on the experimental data to evidence the linearity of the response between sudden drops of load. (For interpretation of the references to colour in this figure legend, the reader is referred to the web version of this article.)

10 times that applied during approach, so that the fibril strains involved are very different. The differences in magnitude notwithstanding, the stiffness during retraction are monotonic with the number of fibrils in contact, just as during approach.

The stiffness of the nanoindenter is 1.4 μN/nm, 35 times larger than the highest stiffness values measured in our experiments. Therefore, the deformation of the force sensor was neglected in the determination of the stiffness values.

Table 1
Average stiffness k_i, for i fibrils in contact with the approaching indenter. The ratio k_i/k_1 is presented to show the deviations from a simple parallel spring model. The values $k_{E=2.15\ \mathrm{MPa}}$ correspond to the stiffness data calculated using the model based on an elastic modulus of E=2.15 MPa. The data are also plotted in Fig. 4.

	Experimental		*Model*
	$k_{average}$ (N/m)	Ratio k_i/k_1	$k_{E=2.15\ \mathrm{MPa}}$ (N/m)
k_1	**7.7**	**1.00**	6.7
SD k_1	**0.3**		
k_2	**13.9**	**1.82**	13.0
SD k_2	**1.1**		
k_3	**16.3**	**2.13**	18.8
SD k_3	**1.7**		
k_4	**24.1**	**3.15**	24.4
SD k_4	**0.9**		
k_5	**26.8**	**3.50**	29.8
SD k_5	**1.2**		
k_6	**31.9**	**4.17**	35.0
SD k_6	**0.8**		
k_7	**38.9**	**5.08**	39.9
SD k_7	**0.3**		

Table 2
Average values for contact stiffness during retraction of the indenter from the surface. The ratio is given with respect to the stiffness of the first fibril in contact during approach, i.e. with respect to the stiffness of one fibril in a low-strain configuration.

Unloading	Average (N/m)	Ratio $k_i/k_1^{approach}$
k_1	**3.8**	**0.49**
SD k_1	**0.126**	
k_2	**7.9**	**1.03**
SD k_2	**0.165**	
k_3	**12.2**	**1.58**
SD k_3	**0.0151**	
k_4	**16.6**	**2.16**
SD k_4	**0.0155**	
k_5	**20.6**	**2.68**
SD k_5	**0.00706**	
k_6	**26.7**	**3.47**
SD k_6	**0.0144**	
k_7	**35.0**	**4.54**
SD k_7	**0.0222**	

4. Elastic deformation of fibrils and backing layer

If the backing layer was rigid, it would not contribute to the deformation and the total combined stiffness of the system would be the sum of the individual stiffnesses of each fibril in contact. With each additional fibril in contact, the stiffness would increase by the same amount. However, the data in Table 1 clearly indicate that the increase in stiffness is less than predicted by the sum of the stiffnesses of the individual fibrils.

In the following, we introduce a model which predicts the stiffness of the PDMS structure as a function of the number of fibrils in contact with the indenter, including the effect of the deformation of the backing layer. The indenter is very stiff and is treated as rigid. This model was first developed by Noderer et al. (2007) and used by them to estimate the stiffness of a large collection of fibrils attached to a rigid indenter. The PDMS structure is treated as a deformable half-space with deformable fibrils (Fig. 2(a)). The fibrils are analyzed as one-dimensional elastic elements subject to infinitesimal strain. The stress in each fibril is considered to be uniform, and applied as traction on a circular patch of the surface of the half-space of PDMS. The displacement of the surface of the half-space of PDMS is computed as the combined effect of all of the fibrils carrying stress (i.e. in contact with the indenter). The displacement of the surface of the PDMS half-space under a given fibril is computed as the effect due to the stress in the given fibril plus the effect of all the other fibrils; the latter contribution is approximated as the displacement of the point on the PDMS half-space at the centre of the fibril. The half-space is assumed to be held motionless far away from the fibrils. Fig. 2(b) shows a cross-section of the deformed surface structure, introducing the parameters used in the following model.

4.1. Elastic response of one fibril

Consider an individual fibril with relaxed height H, radius a, and elastic (Young's) modulus E. Upon applying a tension P that generates an infinitesimal strain in the fibril, it will be elongated by $PH/(\pi a^2 E)$. Now consider the corresponding deformation of the half space. We assume that the stress in the fibril is applied as traction on the surface of the half-space. The half-space deflection caused by such a uniform traction on a circular patch of the surface of the half-space has been given by Johnson (2003). It is sketched in Fig. 2(b). The average upward displacement of the circular patch, i.e. of the bottom displacement, u^b, of the fibril, is $u^b = 16(1-\upsilon^2)'P/(3\pi^2 aE)$. The displacement of the top of the fibril u^t is then the sum of the two contributions

$$u^t = \frac{PH}{\pi a^2 E} + \frac{16(1-\nu^2)P}{3\pi^2 aE} = \left[\frac{H}{(1-\nu^2)a} + \frac{16}{3\pi}\right]\frac{(1-\nu^2)P}{\pi aE} \tag{1}$$

We introduce the compliance, C, of the fibrillar structure, defined as the displacement of the top of the fibrils in contact with the indenter divided by the applied load, and find for one fibril in contact

$$C_{11} = \left[\frac{H}{(1-\nu^2)a} + \frac{16}{3\pi}\right]\frac{(1-\nu^2)}{\pi aE} \tag{2}$$

The stiffness k_1, upon loading one fibril, is the inverse of C_{11}.

4.2. Loading of one fibril—displacement of all other fibrils

Johnson (2003) gives the upward displacement u_z of the surface of the half-space outside of the circular, uniformly loaded patch as

$$u_z = \frac{4(1-\nu^2)P}{\pi^2 aE}\frac{r}{a}\left[J\left(\frac{a}{r}\right) - \left(1-\frac{a^2}{r^2}\right)K\left(\frac{a}{r}\right)\right] \tag{3}$$

where r is the distance from the centre of the fibril, J the complete elliptic integral of the second kind and K the complete elliptic integral of the first kind. We use this to estimate the displacement at the bottom of fibril j when fibril i is loaded, by assuming its value at the centre of fibril j gives its average value, u^b. Designating the bottom displacement of fibril j as u^b_j, we then obtain, due to the loading of a single fibril i,

$$u^b_j = \frac{4(1-\nu^2)P_i}{\pi^2 aE}\frac{s_{ij}}{a}\left[J\left(\frac{a}{s_{ij}}\right) - \left(1-\frac{a^2}{s_{ij}^2}\right)K\left(\frac{a}{s_{ij}}\right)\right] \tag{4}$$

where P_i is the load applied to fibril i and s_{ij} $(i \neq j)$ the distance from the centre of fibril i to the centre of fibril j.

4.3. Multiple loaded fibrils

Now consider the case where n fibrils are loaded. The displacement at the bottom of each fibril will arise due to the effect of the force on each of the loaded fibrils. Consider a loaded fibril, i. The difference in displacement between its top and bottom will be given by

$$u^t_i = u^b_i + \frac{P_i H}{\pi a^2 E} \tag{5}$$

The displacement will be given by the equivalent of Eq. (1) due to the load on fibril i plus a contribution given by Eq. (4) from each of the other loaded fibrils. Therefore,

$$u^t_i = \left[\frac{H}{(1-\nu^2)a} + \frac{16}{3\pi}\right]\frac{(1-\nu^2)P_i}{\pi aE} + \frac{4(1-\nu^2)}{\pi^2 aE}\sum_{j=1,\, j\neq i}^{n} P_j \frac{s_{ij}}{a}\left[J\left(\frac{a}{s_{ij}}\right) - \left(1-\frac{a^2}{s_{ij}^2}\right)K\left(\frac{a}{s_{ij}}\right)\right] \tag{6}$$

re-written as

$$u^t_i = \sum_{j=1}^{n} C_{ij} P_j \tag{7}$$

where

$$C_{ij} = \frac{4(1-\nu^2)}{\pi^2 aE}\frac{s_{ij}}{a}\left[J\left(\frac{a}{s_{ij}}\right) - \left(1-\frac{a^2}{s_{ij}^2}\right)K\left(\frac{a}{s_{ij}}\right)\right] \quad i \neq j \tag{8a}$$

$$C_{ij} = C_{11} = \left[\frac{H}{(1-\nu^2)a} + \frac{16}{3\pi}\right]\frac{(1-\nu^2)}{\pi aE} \quad i = j \tag{8b}$$

The matrix C_{ij} is the compliance matrix for the system of loaded fibrils, giving the same results as derived by Noderer et al. (2007).

4.4. Specific examples for a hexagonal array of fibrils

Consider a hexagonal array of fibrils arranged and numbered as shown in Fig. 1. The numbering indicates the order in which contact is made between the indenter and the fibrils as the indenter is brought towards the fibrillar surface. The order of attachment is caused by the spherical shape of the indenter and the experimental fact that the point on the sphere closest to the surface of the PDMS half-space lies somewhere closer to fibril 1 than to fibrils 2 and 3, and closer to fibril 2 than to 3. The fibril spacing is such that s is the distance from the centre of one fibril to that of a neighbouring one. Note that $C_{ii}=C_{11}$ and $C_{ij}=C_{ji}$ and that for this geometry $C_{12}=C_{13}=C_{14}=C_{23}=C_{24}$ and $C_{34}=C_{25}$ are similar.

In the following, we determine the stiffness $k_i=dF/d\Delta$ of the structure as measured by the indenter with i fibrils in contact where

$$dF=\sum_{j=1}^{i}P_j \text{ and } d\Delta=u_j^t \text{ for all } j\le i$$

For one fibril in contact, we have

$$k_1=\frac{dF}{d\Delta}=\frac{1}{C_{11}} \tag{9}$$

with

$$C_{11}=\left[\frac{H}{(1-\nu^2)a}+\frac{16}{3\pi}\right]\frac{1-\nu^2}{\pi aE}$$

For two fibrils we find that

$$\begin{bmatrix}C_{11} & C_{12}\\ C_{12} & C_{11}\end{bmatrix}\begin{Bmatrix}dP_1\\ dP_2\end{Bmatrix}=\begin{Bmatrix}d\Delta\\ d\Delta\end{Bmatrix} \tag{10}$$

from which we obtain

$$k_2=\frac{dF}{d\Delta}=\frac{dP_1+dP_2}{d\Delta}=\frac{2}{C_{11}+C_{12}} \tag{11}$$

Similarly we proceed for increasing the number of fibrils in contact with the indenter. The results for the stiffness are compiled in Table 3. As a last example, which also indicates the symmetries in the compliance matrix we give the result for

Table 3
Contact stiffness, k_i, as described in the text.

No. of loaded fibrils i	Stiffness k_i
1	$\frac{1}{C_{11}}$
2	$\frac{2}{C_{11}+C_{12}}$
3	$\frac{3}{C_{11}+2C_{12}}$
4	$\frac{4C_{11}-6C_{12}+2C_{34}}{C_{11}^2+C_{11}(C_{12}+C_{34})+C_{12}C_{34}-4C_{12}^2}$
5	$\frac{3(C_{12}+C_{34}-C_{11}-C_{45})(C_{11}-C_{12})+(C_{11}-C_{34})(3C_{12}-C_{34}-2C_{11})}{(C_{11}+2C_{12})(C_{12}+C_{34}-C_{11}-C_{45})(C_{11}-C_{12})+(C_{11}-C_{34})[C_{11}(C_{12}-C_{34})-2C_{12}(C_{11}-C_{12})]}$
6	$\frac{\begin{array}{l}6C_{11}^4-2C_{11}^3(6C_{12}+C_{34}+5C_{45})-C_{11}^2(6C_{12}^2-C_{12}(19C_{34}+22C_{45})+5C_{34}^2-4C_{34}C_{45}-2C_{45}^2)+C_{11}(14C_{12}^3\\ -4C_{12}^2(3C_{34}+2C_{45})-C_{12}(3C_{34}^2+13C_{34}C_{45}+8C_{45}^2)+C_{34}^3+5C_{34}^2C_{45}-2C_{34}C_{45}^2+2C_{45}^3)+2C_{12}^4-2C_{34}^3(8C_{34}+3C_{45})\\ +2C_{12}^2(9C_{34}^2+7C_{34}C_{45}+3C_{45}^2)-C_{12}(4C_{34}^3+9C_{34}^2C_{45}-2C_{34}C_{45}^2+2C_{45}^3)+C_{34}^3C_{45}\end{array}}{\begin{array}{l}C_{11}^5+C_{11}^4(C_{12}+C_{34}-C_{45})-C_{11}^3(8C_{12}^2+C_{12}(2C_{45}-C_{34})+2C_{34}^2+2C_{34}C_{45}+C_{45}^2)+\\ C_{11}^2(2C_{12}^2(3C_{34}+5C_{45})+C_{12}C_{45}(5C_{34}+C_{45})+C_{45}(2C_{34}^2+C_{34}C_{45}+C_{45}^2))+\\ C_{11}(9C_{12}^4-2C_{12}^3(5C_{34}+3C_{45})+C_{12}^2(3C_{34}^2-4C_{34}C_{45}-3C_{45}^2)-C_{12}C_{34}(C_{34}^2+3C_{34}C_{45}+4C_{45}^2)+C_{34}^3C_{45})+C_{12}^2(C_{12}^3\\ -3C_{12}^2(3C_{34}+C_{45})+3C_{12}(3C_{34}^2+2C_{34}C_{45}+C_{45}^2)-C_{34}^3-C_{45}(3C_{34}^2-3C_{34}C_{45}+C_{45}^2))\end{array}}$
7	$\frac{7C_{11}-10C_{12}+2C_{34}+C_{45}}{C_{11}(C_{11}+2C_{12}+2C_{34}+C_{45})-6C_{12}^2}$

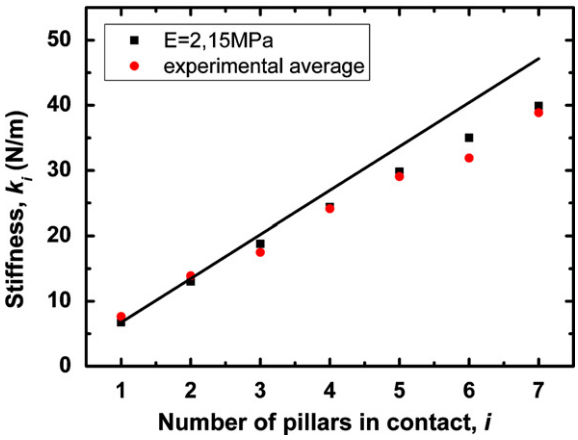

Fig. 5. Stiffness k_i of the combined structure of fibrils and backing as a function of number of fibrils in contact. Circles represent the average of the experimental values and squares the result of the model. An elastic modulus of E=2.15 MPa has been chosen for the model by minimization of the sum of quadratic deviations from experimental stiffness values.

seven fibrils in contact

$$\begin{bmatrix} C_{11} & C_{12} & C_{12} & C_{12} & C_{12} & C_{12} & C_{12} \\ C_{12} & C_{11} & C_{12} & C_{12} & C_{34} & C_{34} & C_{45} \\ C_{12} & C_{12} & C_{11} & C_{34} & C_{12} & C_{45} & C_{34} \\ C_{12} & C_{12} & C_{34} & C_{11} & C_{45} & C_{12} & C_{34} \\ C_{12} & C_{34} & C_{12} & C_{45} & C_{11} & C_{34} & C_{12} \\ C_{12} & C_{34} & C_{45} & C_{12} & C_{34} & C_{11} & C_{12} \\ C_{12} & C_{45} & C_{34} & C_{34} & C_{12} & C_{12} & C_{11} \end{bmatrix} \begin{Bmatrix} dP_1 \\ dP_2 \\ dP_3 \\ dP_4 \\ dP_5 \\ dP_6 \\ dP_7 \end{Bmatrix} = \begin{Bmatrix} d\Delta \\ d\Delta \\ d\Delta \\ d\Delta \\ d\Delta \\ d\Delta \\ d\Delta \end{Bmatrix} \tag{12}$$

and

$$k_7 = \frac{dF}{d\Delta} = \frac{7C_{11} - 10C_{12} + 2C_{34} + C_{45}}{C_{11}(C_{11} + 2C_{12} + 2C_{34} + C_{45}) - 6C_{12}^2} \tag{13}$$

Values for stiffness have been calculated and are compared with experimental results in Table 1 and in Fig. 5. The only adjustable parameter is the elastic modulus E, with the assumption that ν=0.5 is an appropriate value for the Poisson ratio of PDMS. The elastic modulus has been determined to be E=2.15 $\pm$ 0.10 MPa by minimization of the sum over k_1–k_7 of quadratic deviations from experimental averages.

4.5. Further approximations

If we neglect the interactions other than with the nearest neighbour fibrils, we obtain significantly simpler expressions than those derived above. The results are obtained by setting all compliances to zero other than C_{11} and C_{12}. This approximation should be valid when the spacing between fibrils is significant compared to their diameter, which is however not the case in the system presented in this paper.

5. Discussion

In this section we discuss our experimental data and compare the results of our model. We proceed chronologically through the events observed as the indenter approaches the structured surface and is retracted from it.

The indenter approaches the sample surface starting from a distance at which no force is detected between it and the indenter. The first significant deviation from zero force is a sudden drop in load when the first fibril makes contact with the indenter; see Fig. 4, where this event is marked with the no. 1. The first contact always results in a tensile force, evidencing attractive forces between indenter and fibrils. The linear increase of the force after its drop yields a value for the stiffness of the sample and the nanoindenter load cell combined when one fibril is attached to the sphere. The average value from several experiments is k_1=7.7 N/m, almost two-orders of magnitude lower than the stiffness of the load cell. We conclude that the jump into contact of the first fibril occurs through a sudden stretching of the fibril plus deformation of the backing, with negligible motion contributed from the load cell. The net displacement can be calculated as the force drop divided by the stiffness k_1, and regarded as the deformation of the fibril and the backing layer combined. The resulting values vary between

190 and 450 nm, i.e. the typical strain in the fibril after the first jump into contact is of the order of 2%, an estimate we obtain by ignoring the deformation of the backing layer.

Zero depth in Figs. 3 and 4 has been chosen retroactively to be the sphere's location when it is attached to one fibril at zero load. This calibration is achieved by extending the straight line in Fig. 4 that denotes the system response after load drop 1, and by doing so until the extension passes through zero load, which is then defined as the origin of the graph. This choice for zero depth reflects the position of the indenter where one fibril in contact would be unstrained on average. Due to the surface curvature of the indenter and the fact that the lowest point on it is not guaranteed to be located exactly over the centre of fibril 1 (see Figs. 1 and 2), this zero depth differs from the sphere position where a perfectly rigid fibril would make first contact with the indenter by up to 36 nm, given by the height variation of the spherical indenter across the 5 μm radius of the fibril.

The deduced range of the attractive interaction (154–450 nm) is significantly larger than expected for pure van der Waals attraction. There is debate regarding the forces acting in micro-structured adhesive systems, addressing whether they are mainly van der Waals forces (Autumn, 2006; Autumn et al., 2002) or include other contributions like capillary forces (Huber et al., 2005). Our results strongly indicate that long-range electrostatic forces have to be considered for the case of PDMS interacting with sapphire. This conclusion is confirmed by preliminary results for the experiment repeated with both indenter and sample immersed in water. In water we observe no initial jump into tension when the indenter makes contact with the fibrils during approach, but the same discrete detachment of fibrils occurs in tension during retraction. These results suggest that an electrostatic attraction between sapphire and PDMS present in air has been screened by the water when the experiment is carried out in the submersed condition.

Returning to the sequence of events that occur during indenter approach in air, we consider Fig. 4 further. The jump-into-contact events recur in time as the indenter moves toward the sample and the number of fibrils in contact increases. At a certain indenter position, the force sensed by the indenter will change from tension to compression since the stretching of the latest fibrils into contact is compensated by the compression of the earlier attached fibrils. The force vs. depth curve becomes steeper with each additional fibril in contact, reflecting the expected increase in stiffness. The linearity of the section in between force drops indicates that each fibril immediately makes complete contact. Such increase of contact area in well-defined steps is very helpful for the quantitative evaluation of elasticity parameters. In our system, the gain in adhesion energy is large enough to elastically stretch and deform the fibrils such that full contact is established once the fibrils come close to the indenter. This observation is a clear demonstration of the enhancement of contact formation by micro-structuring surfaces, a core concept of fibrillar biomimetic adhesive materials.

The stiffness increases sublinearly with the number of fibrils in contact. Our model explains this trend taking into account the deformation of the backing layer. Fig. 5 compares the experimental k_i values with the model data. The straight line represents the stiffness assuming a rigid backing layer. The model correctly predicts the stiffness relations. The only adjustable parameter is the elastic modulus E. It was found, by minimizing the sum of the squares of the differences between the model and the averaged experimental k_i data, to be $E=2.15\pm0.10$ MPa, as stated above. Note that the combination of our experimental method and our model allows for the unique determination of the elastic modulus of PDMS fibrils within a given micro-structure *in situ*. The elastic modulus of PDMS polymers similar to our material has been determined by a variety of methods and values scatter between 1.3 and 4 MPa (Bar et al., 1999; Deuschle et al., 2008; Gupta et al., 2006; Schneider et al., 2008; Song et al., 2008). Our method avoids the contact size problems usually encountered in indentation of flat elastomer samples (Deuschle et al., 2008; Ebenstein and Wahl, 2006) and takes into account possible variations of the elastic modulus for a material which is cured in a confined geometry.

The formulae describing the stiffness for several fibrils in contact could be simplified if only interactions between nearest neighbour fibrils would be considered. Such simplification would set to zero all compliances other than C_{11} and C_{12}. However, an analysis of the relative contributions shows that this is not a valid approximation for fibril structures in which the distance between fibrils is comparable to their diameter. In our structure, the displacement of the first-loaded fibril, u_{11}, is 28 times higher than that of the nearest first neighbour, u_{12}, but the displacement of the second nearest neighbour, u_{34} is still half of that of the first neighbour, u_{12}.

Upon retraction of the indenter, a significant adhesion hysteresis is observed in Fig. 3. The seven fibrils are detached one after the other. However, detachment of the first of seven fibrils occurs only far into the tensile regime. The highest attractive force of about 100 μN is encountered with four fibrils in contact and the indenter about 5 μm above where the undeformed surface would be, i.e. under a strain in the fibrils of approximately 25% if we neglect the deformation of the backing. The force vs. distance curve during retraction is step-wise linear between the force jumps, similar to the approach. The values for the stiffness decrease monotonically with decreasing number of fibrils in contact; they are listed in Table 2. Note that Table 2 indicates that the stiffness of the system during retraction with only 1 or 2 fibrils attached is significantly lower than that for the approach with the same number of fibrils in contact. The difference in compliance between retraction and approach with just one or two pillars in contact seems to be largely due to the fibril strain in each case, namely 25–35% during retraction, but only a few percent during approach. Therefore, to investigate the compliance difference between retraction and approach, we estimate the system stiffness just prior to detachment of the last fibril taking into account the finite strain. We model the material as an incompressible Mooney rubber (Treloar, 2005). The Mooney formulation of the strain energy density allows for Gaussian chain elasticity constrained by chemical cross-links and entanglements, where the entanglements evolve and gradually release under tension. Although the model has its deficiencies in compression and at large stretches, it is reasonably reliable at modest strains under tension (Treloar, 2005). The derivation of our estimate is presented in the Appendix. We find a stiffness of the system of 4.2 N/m just before the last

fibril detaches, significantly lower than the small strain stiffness when one fibril is attached, as recorded in Table 1. Consulting Table 2, we find that the measured stiffness for the system when there is only one fibril left attached is 3.8 N/m, only 10% off the predicted value. However, we can expect that finite strain effects in the backing layer of PDMS near the bottom of the fibril will contribute a further reduction of the stiffness, an effect we have ignored in our model.

Finally, we briefly discuss the adhesion properties of our sample although that is not the focus of this article. In Fig. 3, the shape of the adhesion hysteresis for the fibril structure resembles the curve measured on a flat PDMS surface. While the maximum tensile force during retraction is similar, the adhesion hysteresis is larger by a factor of approximately three, emphasizing once more the function of the microstructure in terms of the adhesive properties. A quantitative analysis shows that the average nominal stress transmitted through the contacting fibrils at maximum tension is just over 5 times the stress on the JKR contact (Johnson et al., 1971) between the sphere and the flat PDMS surface at its maximum tension. We recognize that the stress on a JKR contact is not always a meaningful measure of the effectiveness of its adhesion, but we quote it to enable comparison on a specific basis relative to the fibrillar surface. This result illustrates the adhered, structured surface's superior ability to transmit tension.

In the absence of detachment defects, frictionless flat punch contacts show a strong resistance against peeling as there is no stress singularity at the edge as in sphere-on-flat situations. Similarly, when the more realistic case of a flat punch contact with friction is considered, also in the absence of detachment defects, the driving force for detachment is low compared to the JKR setup of the sphere on a flat (Ebenstein and Wahl, 2006; Spuskanyuk et al., 2008). We believe that this feature is responsible for the tenacity of the fibrillar adhesion exhibited by the structured surface. Additionally, the strength of adhesion compared to the softness of the fibrils at the micrometer scale yields perfectly flat contacts, enabling accommodation of a degree of surface roughness without detachment defects.

6. Conclusions

In conclusion, we have performed contact mechanics experiments on a fibrillar micro-structured PDMS surface. Attachment and detachment of individual fibrils have been detected in force and stiffness measurements. Small deformations during approach of an indenter have been quantitatively modelled taking into account deformation of both the fibrils and the backing layer. The results emphasize the importance of long-range interactions via the substrate for the contact mechanics of elastic materials. The discrete growth of the contact area with increasing number of fibrils in contact allows an accurate *in situ* determination of the elastic modulus of the PDMS to be 2.15 MPa.

Appendix

In order to understand the comparatively low stiffness values found for the last fibrils in contact during retraction, we model the deformation of one fibril in contact including the effects of finite strain. As before, we assume the fibril is deforming in uniaxial stress, so that the stress and strain are uniform. The material is modelled as an incompressible Mooney rubber having strain energy density per unit mass (Treloar, 2005)

$$\frac{W}{\rho}=\frac{E}{12\rho}\left(\lambda_1^2+\lambda_2^2+\lambda_3^2+\frac{1}{\lambda_1^2}+\frac{1}{\lambda_2^2}+\frac{1}{\lambda_3^2}-6\right) \tag{A1}$$

where ρ is the density and λ_i, i=1,2,3, are the orthogonal principal stretch ratios. By incompressibility $\lambda_1\lambda_2\lambda_3=1$. In the form chosen for (A1), the two conventional constants for the Mooney rubber have been set equal to each other as a special case. Normally the ratio of these constants would be determined by the degree of entanglement versus the density of chemical cross-links. In the absence of such information the ratio has been chosen as unity.

The nominal stress components, T_i, in the axial direction and one transverse direction are given by

$$T_3=\frac{\partial W}{\partial\lambda_3}-\frac{p}{\lambda_3}=\frac{E}{6}\left(\lambda_3-\frac{1}{\lambda_3^3}\right)-\frac{p}{\lambda_3} \tag{A2a}$$

$$T_1=\frac{\partial W}{\partial\lambda_1}-\frac{p}{\lambda_1}=\frac{E}{6}\left(\lambda_1-\frac{1}{\lambda_1^3}\right)-\frac{p}{\lambda_1}=0 \tag{A2b}$$

where p is the hydrostatic pressure in the material. The transverse stress has been set to zero consistent with the conditions in the fibril, allowing the pressure to be calculated and inserted into Eq. (A2a), providing

$$T=\frac{E}{6}\left(1+\lambda-\frac{1}{\lambda^2}-\frac{1}{\lambda^3}\right) \tag{A3}$$

where the subscript indicating the axial direction has been dropped. To obtain Eq. (A3), we have used axial symmetry so that $\lambda_1=\lambda_2$, and then invoked incompressibility in the form $\lambda_1^2=1/\lambda_3$. Note that at a stretch ratio λ=1.24 and with E=2.15 MPa, the nominal stress from Eq. (A3) is 0.38 MPa. Given the cross-sectional area of the fibril, equal to 0.79×10^{-10} m^2, this gives an axial load on the fibril equal to 30 μN, consistent with the tensile load at which the last fibril detaches (Fig. 3).

The displacement of the top of the one attached fibril may now be estimated as

$$u_t = H(\lambda - 1) + u_b \tag{A4}$$

a formula equivalent to Eq. (1) but without specialization to infinitesimal strain. We now assume that the displacement of the bottom of the fibril can still be computed from infinitesimal strain theory, so that we obtain

$$u_t = H(\lambda - 1) + \frac{16(1-\nu^2)P}{3\pi^2 aE} \tag{A5}$$

After differentiation of Eq. (A5) with respect to u_t, we obtain an expression for the stiffness of the system in the form

$$\frac{dP}{du_t} = \frac{\pi aE}{H/a/d(T/E)/d\lambda + 16(1-\nu^2)/3\pi} \tag{A6}$$

where we have used the relationship $P=\pi a^2 T$, consistent with the definition of nominal stress, in order to express $d\lambda/du_t$ through dP/du_t. Eq. (A3) provides us with

$$\frac{d(T/E)}{d\lambda} = \frac{1}{6}\left(1 + \frac{2}{\lambda^3} + \frac{3}{\lambda^4}\right) \tag{A7}$$

Note that when $\lambda=1$, $d(T/E)/d\lambda=1$, consistent with conditions at infinitesimal strain. We now investigate the predictions of Eq. (A6), with $\nu=½$ for incompressibility, $H/a=3.74$ as in the experiments, and $E=2.15$ MPa as calibrated to those same experiments. For fibrils having a radius $a=5$ μm as in the experiments, the stiffness from Eq. (A6) when the strain is infinitesimal (i.e. $\lambda=1$) is given by 6.7 N/m as used for the model result for the single fibril case in Table 1. Just before the last fibril detaches, when $\lambda=1.24$, we find that Eq. (A7) predicts that $d(T/E)/d\lambda=0.55$, and the stiffness of the system from Eq. (A6) is 4.19 N/m. This prediction is discussed in Section 5.

References

Arzt, E., Gorb, S., Spolenak, R., 2003. From micro to nanocontacts in biological attachment devices. Proc. Natl. Acad. Sci. 100 (19), 10603–10606.
Autumn, K., 2006. How Gecko toes stick. Am. Sci. 94, 124–132.
Autumn, K., 2007. Gecko adhesion: structure, function, and applications. MRS Bull. 32, 473–478.
Autumn, K., Liang, Y.A., Hsieh, S.T., Zesch, W., Chan, W.P., Kenny, T.W., Fearing, R., Full, R.J., 2000. Adhesive force of a single gecko foot-hair. Nature 405, 681–685.
Autumn, K., Sitti, M., Liang, Y.A., Peattie, A.M., Hansen, W.R., Sponberg, S., Kenny, T.W., Fearing, R., Israelachvili, J.N., Full, R.J., 2002. Evidence for van der Waals adhesion in gecko setae. Proc. Natl. Acad. Sci. 99 (19), 12252–12256.
Bar, G., Delineau, L., Brandsch, R., Bruch, M., 1999. Importance of the indentation depth in tapping-mode atomic force microscopy study of compliant materials. Appl. Phys. Lett. 75 (26), 4198–4200.
Boesel, L.C., Greiner, C., Arzt, E., DelCampo, A., 2010. Gecko-inspired surfaces: a path to strong and reversible dry adhesives. Advance Materials 22 (19), 2125–2137.
Del Campo, A., Arzt, E., 2008. Fabrication approaches for generating complex micro- and nanopatterns on polymeric surfaces. Chem. Rev. 108, 911–945.
Del Campo, A., Greiner, C., Arzt, E., 2007. Contact shape controls adhesion of bioinspired fibrillar surfaces. Langmuir 23 (20), 10235–10243.
Deuschle, J.K., Buerki, G., Deuschle, H.M., Enders, S., Michler, J., Arzt, E., 2008. In situ indentation testing of elastomers. Acta Mater. 56, 4390–4401.
Ebenstein, D.M., Wahl, K.J., 2006. A comparison of JKR-based methods to analyze quasi-static and dynamic indentation force curves. J. Colloid Interface Sci. 298, 652–662.
Gao, H., Yao, H., 2004. Shape insensitive optimal adhesion of nanoscale fibrillar structures. Proc. Natl. Acad. Sci. 101, 7851–7856.
Gorb, S., Varenberg, M., Peressadko, A., Tuma, J., 2007. Biomimetic mushroom-shaped fibrillar adhesive microstructure. J. R. Soc. Interface 4, 271–275.
Greiner, C., del Campo, A., Arzt, E., 2007. Adhesion of bioinspired micropatterned surfaces: effects of pillar radius, aspect ratio, and preload. Langmuir 23 (7), 3495–3502.
Gupta, S., Carrillo, F., Li, C., Pruitt, L., Puttlitz, C., 2006. Adhesive forces significantly affect elastic modulus determination of soft polymeric materials in nanoindentation. Proc. Natl. Acad. Sci. 61, 448–451.
Huber, G., Mantz, H., Spolenak, R., Mecke, K., Jacobs, K., Gorb, S.N., Arzt, E., 2005. Evidence for capillarity contributions to gecko adhesion from single spatula nanomechanical measurements. Proc. Natl. Acad. Sci. 102 (45), 16293–16296.
Hui, C.-Y., Glassmaker, N.J., Tang, T., Jagota, A., 2004. Design of biomimetic fibrillar interfaces: 2 mechanics of enhanced adhesion. J. R. Soc. Interface London, 35–48.
Johnson, K.L., 2003. Contact Mechanics. Cambridge, (UK).
Johnson, K.L., Kendall, K., Roberts, A.D., 1971. Surface energy and the contact of elastic solids. Proc. R. Soc. Lond. A 324, 301–313.
Kamperman, M., Kroner, E., Campo, A.d., McMeeking, R.M., Arzt, E., 2010. Functional surfaces with 'Gecko' effect: from principles to application. Adv. Eng. Mater.
Kim, S., Sitti, M., 2006. Biologically inspired polymer microfibers with spatulate tips as repeatable fibrillar adhesives. Appl. Phys. Rev. Lett. 89, 261911–261913.
Kim, S., Sittia, M., Hui, C.-Y., Long, R., Jagota, A., 2007. Effect of Backing Layer Thickness on Adhesion of Single-level Elastomer Fiber Arrays 91, 161903–161905.
Lee, H., Lee, B.P., Messersmith, P.B, 2007. A reversible wet/dry adhesive inspired by mussels and geckos. Nature 448, 338–341.
Long, R., Hui, C.-Y., 2009. The Effect of Preload on the Pull-off Force in Indentation Tests of Microfibre Arrays 465, 961–981.
Long, R., Hui, C.-Y., Kim, S., Sitti, M., 2008. Modeling the soft backing layer thickness effect on adhesion of elastic microfiber arrays. J. Appl. Phys. 104 044301/044301–044309.
Majumder, A., Sharma, A., Ghatak, A., 2010. Bio-inspired adhesion and adhesives: controlling adhesion by micro–nanostructuring of soft surfaces. In: Chakraborty, S. (Ed.), Microfluidics and Microfabrication. Springer, USA, pp. 283–307.
McMeeking, R.M., Arzt, E., Evans, A.G., 2008. Defect dependent adhesion of fibrillar surfaces. J. Adhes. 84, 675–681.
Noderer, W.L., Shen, L., Vajpayee, S., Glassmaker, N.J., Jagota, A., Hui, C.-Y, 2007. Enhanced Adhesion and Compliance of Film-terminated Fibrillar Surfaces 463, 2631–2654.
Peressadko, A., Gorb, S.N., 2004. When less is more: experimental evidence for tenacity enhancement by division of contact area. J. Adhes. 80, 247–261.
Persson, B., 2001. Theory of rubber friction and contact mechanics. J. Chem. Phys. 115 (8), 3840–3861.
Schneider, F., Fellner, T., Wilde, J., Wallrabe, U., 2008. Mechanical properties of silicones for MEMS. J. Micromech. Microeng. 18, 065008–0650017.
Song, J., Tranchida, D., Vancso, G.J., 2008. Contact mechanics of UV/ozone-treated PDMS by AFM and JKR testing: mechanical performance from nano- to micrometer length scales. Macromolecules 41, 6757–6762.
Spuskanyuk, A.V., McMeeking, R.M., Deshpande, V.S., Arzt, E., 2008. The effect of shape on the adhesion of fibrillar surfaces. Acta Biomater. 4, 1669–1676.
Sun, W., Neuzil, P., Kustandi, T.S., Oh, S., Samper, V.D., 2005. The nature of the Gecko lizard adhesive force. Biophys. J.: Biophys. Lett. 89 (2), L14–L17.
Treloar, V.L.R.G., 2005. In: The Physics of Rubber Elasticity. Oxford University Press, New York (USA).